AERODYNAMIC DESIGN OF SOLAR ENERGY CARS FOR AUSTRALIAN AND CHILEAN RACE COMPETITIONS

Pablo Pacheco, Daniel Garrido, Nelson Moraga, Alejandro Abarcia

Departamento de Ingeniería Mecánica, Universidad de La Serena, Benavente 980, La Serena-Chile

Abstract

This paper presents the aerodynamic design of three and four wheeled solar cars that had the leading positions in Atacama Solar Race, Chile in 2012, 2013 and 2014 and in the World Solar Challenge, Australia, 2013. Fluid mechanics governing equations for air turbulent flow around the cars were solved with pertinent RANS turbulent models by using the Finite Volume Method. The sequence of the development of three solar cars, IK1 and IK2 with three wheels and the four wheeled IK3 is described with details of the design in a virtual air tunnel. Data of solar energy irradiation, wind magnitude and direction and air temperature in Chilean and Australian races are used in the design process. The energy consumption of each car model is predicted for the 3,000 km race in Australia. The sequential calculation procedure based on numerical simulation of the turbulent air flow around each solar car prototype at 90 km/hr allowed a reduction of 3% in the frontal area and of 13% in the drag coefficient from IK1 to IK2 three wheeled cars and a reduction of 22% in the front area and 41% in the drag coefficient from IK2 to IK3 with four wheels. Major solar energy consumption at 90 km/hr is due to drag forces, accounting to 85%, followed by rolling forces (13.5%).

Keywords: Solar cars. Aerodynamic design. Photovoltaic cells. Power consumption. CFD simulations.

1. Introduction

One third of the world energy consumption is in transportation, currently based mainly on the use of fossil fuels accounting for carbon, unburned fuel, nitrate oxides and sulfur oxides harmful emissions. The use of suitable energy sources for transportation is a major concern all around the world. One of the appropriated developing technologies is based on the use of solar energy for ground transportation (Vinnichenko et al. 2014).

The development of electrical solar cars can contribute to reduce fossil fuel consumption responsible for combustion dangerous emissions (Ajanovic 2014) while at the same time it is a public display of one potential technological application of solar energy (Flores-Sánchez et al. 2014). The interesting attempt to develop solar car construction projects with students has been reported by Wellington (1996). The development of lighter and more efficient photovoltaic cells to be used in transportation vehicles (Fattori et al. 2014) has been tested in a hybrid car with an important reduction in gas emissions, as described by Giannouli and Yianoulis (2012). Changes on temperature in a moving vehicle can cause losses in the solar energy being captured by the photovoltaic cells that can be attenuated by an algorithm designed to maximize the energy being stored in batteries, Huang and Chao (2012). A lack of technical information available on the design of solar racing cars has been explained by the

Nomenclature

A	frontal area (m^2)
C_{ai}	constants of the transport equation for the intermittency
C_d	drag coefficient
C_{s1}	constant of the separation-induced transition equation
$C_{\gamma i}$	constants for the intermittency equation
$C_{\Theta t}$	constant for the transition momentum thickness Reynolds number
$E_{\gamma i}$	relaminarization terms in Transition SST model $(kg/m^3/s)$
f	rolling coefficient
F_D	drag force (N)
F_g	gravitational forces (N)
F_{length}	function to control transition length
F_{onset}	function to control transition onset location
F_r	rolling force (N)
$F_{reattch}$	function of the separation adaptation of the Transition SST model
F_{turb}	function of the transition SST model
F_{wake}	function of the transition SST model
F_{θ_t}	blending function of the source term of the Transition SST model
g	acceleration of gravity (m/s^2)
G_k^*	production source term in the k equation $(kg/m/s^3)$
k	turbulent kinetic energy (m^2/s^2)
m	mass of the car (kg)
$P_{\gamma \mathrm{i}}$	transition source terms $(kg/m^3/s)$
$P_{\theta t}$	production source term $(kg/m^3/s)$
Re	Reynolds Number
R_T	turbulent Reynolds number
Re_V	strain-rate Reynolds number
Re_{θ_C}	momentum thickness Reynolds number where the intermittency starts to increase
Re_{θ_t}	momentum thickness Reynolds number where the skin friction starts to increase
$R\tilde{e}_{\theta_t}$	transported variable for Re_{θ_t}
Re_ω	turbulent Reynolds number in functio of omega
S	strain rate magnitude $(1/s)$
S_k	source term in k equation $(kg/m/s^3$
t	time (s)
U	free stream velocity (m/s)
U_j	cartesian velocity components (m/s)
x_j	cartesian coordinates (m)
Y_k^*	destruction source term in the k equation $(kg/m/s^3)$
y	wall-normal distance (m)
α	slope of the road (rad)
γ	intermittency
γ_{eff}	effective intermittency
Γ_k	turbulent diffusivity $(kg/m/s)$
γ_{sep}	separated intermittency
δ	boundary layer thickness (m)
δ_{BL}	function for the source term calculation in the transition momentum thickness Reynolds number transport equation
ε	rate of turbulent energy dissipation(m^2/s^3)
θ_{BL}	function for the source term calculation in the transition momentum thickness Reynolds number transport equation
μ	dynamic viscosity $(kg/m/s)$
μ_t	turbulent viscosity $(kg/m/s)$
ρ	density (kg/m^3)
σ_γ	constant for the intermittency equatio
ω	specific dissipation rate $(1/s)$
Ω	vorticity magnitude $(1/s)$

attitude of the competitors that keep avoiding to share their developments, Kieffer et al. (2006). However, the development of the car winner of the World Solar Challenge (WSC) of 1987, Sunraicer by General Motors was published by King (1991) and by Hampson et al. (1991). A detailed information on the aerodynamic design and construction of Dream, the winner of WSC in 1996 was reported by Ozawa et al. (1998).

Numerical simulations are currently used in aerodynamic vehicle designs (Muyl et al. 2004, Lehmkuhl et al. 2013). Craparo and Thacher (1995) described a mathematical model and the numerical simulation code developed to predict the dynamics of a solar car that included the effects of solar irradiation and temperature on thermal efficiency. Vehicle dimensions and typical transportation velocities cause air flow around the vehicles be turbulent. Three is the number of turbulence families of models: Direct Numerical Simulations (DNS), Jiménez (2003), Large Eddy Simulations (LES), Sagaut (2001) and Reynolds Averaged Navier-Stokes (RANS) models, Chen and Jaw (1998). DNS of a three-dimensional turbulent flow in a channel with a Reynolds number equal to 100,000 required the use of a grid of the order of 8×10^9 nodes, and 6 months for a typical computations on the 'Mare Nostrum' supercomputer on 2100 processors in Barcelona, Hirsh (2007). LES reduces the total computation effort, proportional to Re^3 required in DNS, to $Re^{9/4}$, that still is excessively high for the large Reynolds numbers found in solar race cars. A suitable RANS model with four additional equations to continuity and linear momentum for studying air turbulent flows around cars is the Transition Shear Stress Transport model (Transition SST), Langtry and Menter (2005), Menter et al. (2003).

The aerodynamic study of the Belgium solar car that run in WSC 2009 was done in a wind tunnel and by RANS numerical simulations. The use of the Transition SST turbulent model with a grid of the order of 1.9×10^7 nodes reduced to 3% the error in the calculation of the drag force, from the 18% calculated with the κ-ϵ turbulent model as reported by a comparison with experimental data in a wind tunnel, van Duppen (2010). Fluid mechanics insights such as the large size turbulence structure have been described with LES using seven millions nodes by Tsubokura et al. (2009). Turbulent air flow with *Re* = 900,000 around a simplified car model was studied using 20 million nodes with a EASM model requiring 4,200 hours of computing time and a DES-SST model with a grid of 10.8 million nodes and 5,000 hours of CPU, Guilmineau et al. (2013). Ahmed et al. (2013) characterized the aerodynamic of a geometrical simple approximation of a car using the Unsteady Reynolds Averaged Navier-Stokes Equations (URANSE) model by a 2.7 million nodes grid, with the conclusion that most RANS model can produce coefficient with errors in the interval between 4 and 20%.

The effect of lateral winds on vehicles have been characterized by using *LES* for a freight wagon by Hemida et al. (2010). Tsubokura et al. (2010) described the influence of a sinusoidal crosswind imposed on a lateral boundary of a 1/20 scaled car at Re = 20,000 with LES, with a grid made of 4 million nodes and a time step equal to 5×10^{-6} s. A similar study with the LES turbulent model was done for a simplified model of a train (Re = 22,615) with a mesh of 17.3 million nodes, Krajnovic et al. (2012). Transient aerodynamic simulations of vehicles have been used to calculate forces (Corin et al. 2008) and the prediction of winds on vehicle motion (Nakashima et al. 2013).

The objective of this paper is to describe the aerodynamic design of a series of three solar racing cars developed at the Universidad de La Serena, Chile, that have participated successfully in races of solar cars in Chile in 2011, 2012 and 2014 and in one world competition in Australia in 2013. The evolution of the designs included the change of the use of three wheels for the two first models to four wheels in the last model, the continuous replacement of higher efficient light solar cells, change of

structural materials with lower weights, major changes in the battery cooling system and improved geometrical shape on each new model. The design process was mainly accomplished in virtual wind tunnels in which the fluid mechanics of the turbulent flow of air around the car was carefully predicted with suitable RANS turbulent models, analyzed and used to reduce frontal area and friction losses to minimize aerodynamic drag for each new model. The change of the driver seat from the center of the car to one of the sides was decided after a computational fluid mechanics study of the effect of lateral wind was accomplished.

2. Solar energy racing cars

Three successive models of solar cars have been designed at Universidad de La Serena (ULS), Chile since 2011. IK1 was the first solar car built at ULS with three wheels, the driver located at the center of the car, made of glass fiber and a chrome-molibdenum alloy. The IK1 was the winner of the Atacama Solar Challenge (ASC), the 2011 Latin-American solar race in Atacama Desert, Chile. The second version (IK2) had the same design but a chassis made of carbon fiber and a 7075 aluminum suspension, that was the winner of the 2012 ASC in Chile and it was the runner up on the Adventure category of the 2013 World Solar Challenge (WSC) in Australia. The third model (IK3) was designed to run in Chile in ASC 2014, with a lower number of carbon fibers, an improved aerodynamic design and the pilot located at one of the sides of the car.

The energy required for each car is obtained from the sun irradiation. The first car of the series, IK1 used poly-crystalline photovoltaic cells, with 14% of thermal efficiency, capable of capturing the solar radiation regardless of the inclination of the incident sun rays. The second model, IK2, was built with single crystal silica C-60 Sunpower photovoltaic cells made in Germany, with an increased thermal efficiency of 22%. Photovoltaic E-60 Sunpower cells, developed with a micro-pyramidal surface of 5 µm in high allowed to achieve a 24% of thermal efficiency in the third sun powered IK3 car. The arrays of the photovoltaic cells for each one of the three solar racing cars developed at ULS are shown in Fig.1.

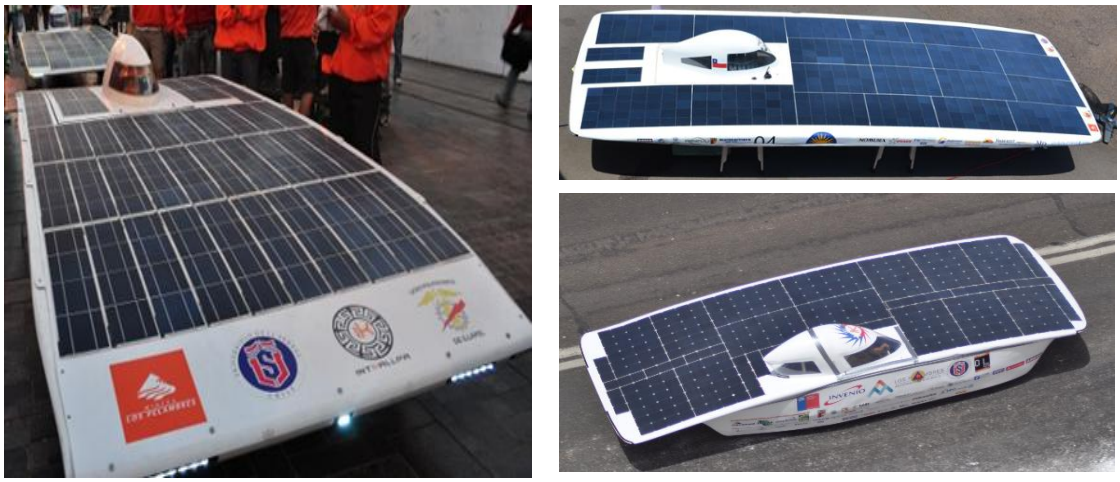

Fig.1. IK1 (left), IK2 (high right) and IK3 (bottom right) solar cars.

The sequential design process included the test of each car at least in a major solar race. A precise knowledge of the places were the cars must run is very important before the design of the car is started. Three of the competition sites were located in the north of

Chile, in the Atacama Desert in which the 2014 route had a length of 1100 km, for a competition of four days, as shown in Fig. 2. The cars must run by the Pacific Ocean, at 30 m of high, then in the desert at 1050 m high and climbed up to 4500 m high near the Andes Mountains. Solar radiation during the 2014 Atacama Solar Race was between 625 to 1050 W/m^2, being lower at Calama and higher at Toconao. Ambient temperature reached values of 28°C in Calama and increased to 35°C in Toconao as indicated in Fig. 2.

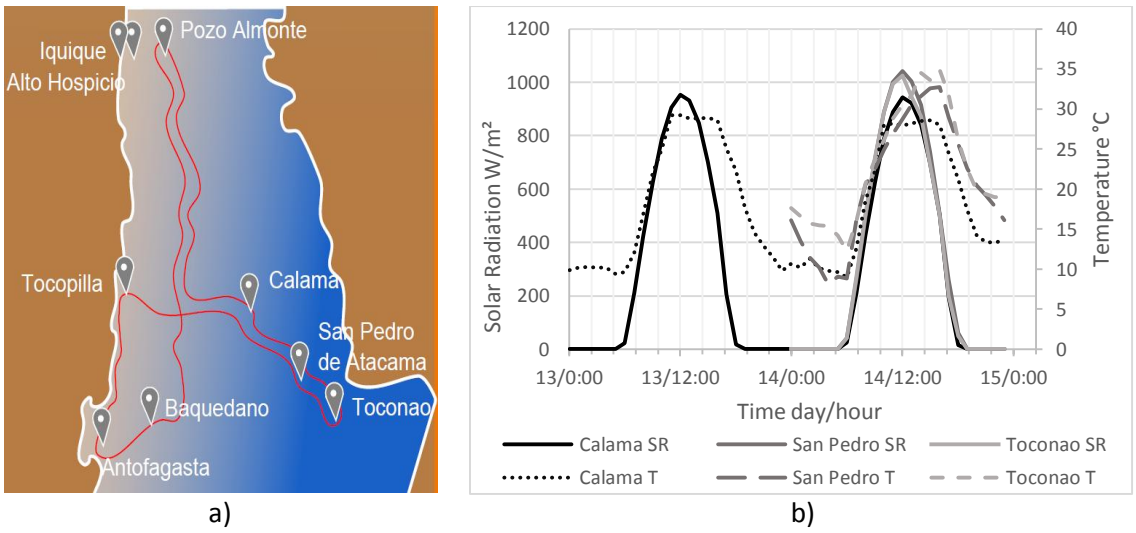

Fig.2. (a) Route of 2014 Solar Atacama Race; (b) solar radiation and air temperature.

Knowledge of the information about wind velocity and wind directions is relevant in the design of solar racing cars. Fig. 2 describes that wind velocities are low in Chile during ASR, with higher expected values of 14 km/hr at the higher locations near the Andes Mountains (Toconao).

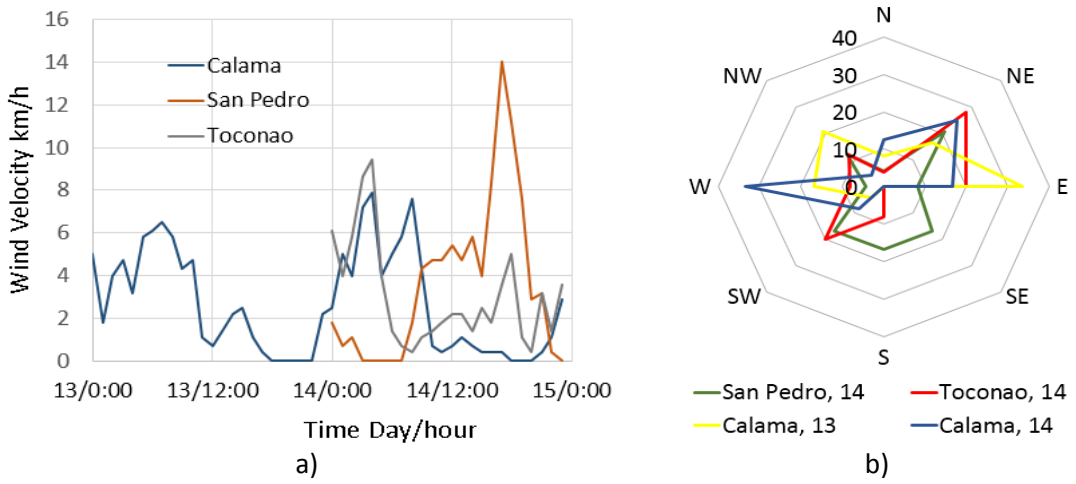

Fig. 3. Wind velocity (a) and wind direction in % (b) expected in 2014 ASR Chile.

World Solar Challenge in 2013 was from Darwin to Adelaide in Australia with a length of 3,000 km. Fig. 4 shows that the route has few curves and its high increases slowly from sea level up to 750 m at the mid distance and then decreases in a soft fashion to the sea level at the end.

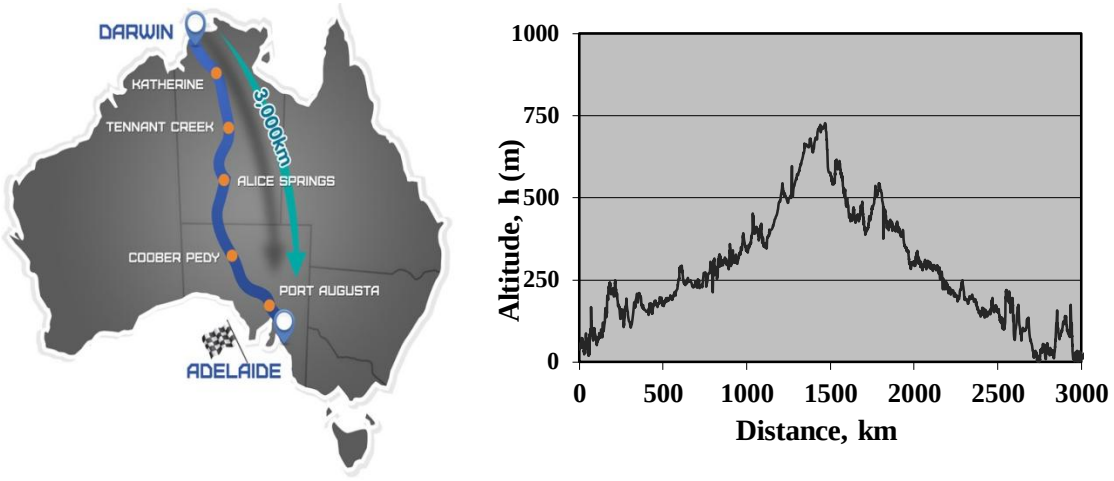

Fig. 4. Route of 2013 WSC at Australia (left) and altitude over sea level (right).

Averaged values of wind velocity and wind direction in the cities of Darwin, Alice Springs and Adelaide, Australia, are presented in Fig. 5. Wind with velocities over 20 km/hr, with higher values of 40 km/hr are expected to be found in the World Solar Challenge in Australia.

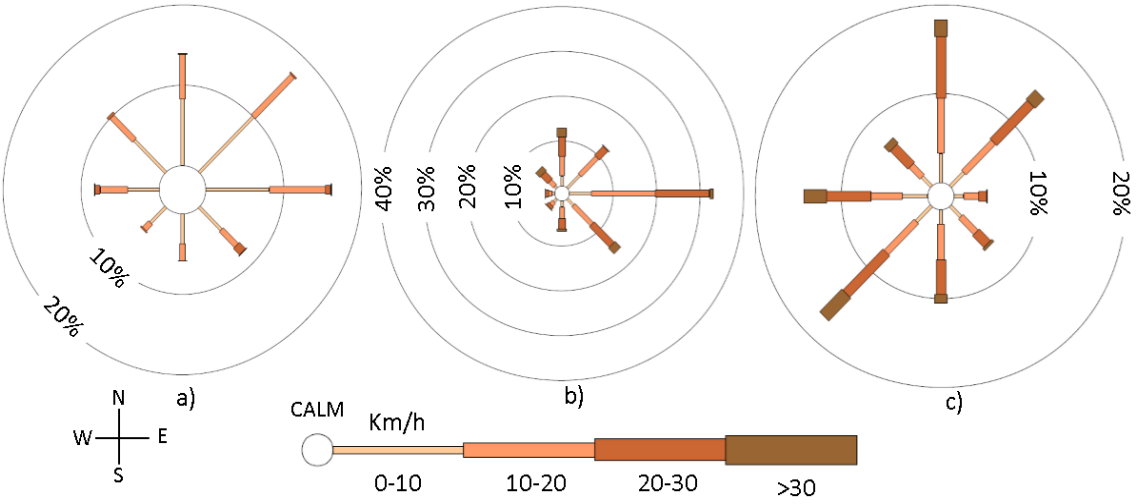

Fig. 5. Wind direction and velocity at: a) Darwin, b) Alice Springs y c) Adelaide in WSC Australia.

3. Aerodynamic Mathematical Model

Fluid mechanics of the turbulent air flow around each one of the three solar racing cars was predicted using the finite volume method. The mathematical model was based on the continuity, three-dimensional linear momentum equations and the standard κ-ϵ turbulent model for the two first models: IK1 and IK3. The aerodynamic design of the third car of the series, IK3, was accomplished by using the transition SST turbulent

model, as described by Langtry and Menter (2005). The four additional equations of the Transition SST model are presented below. The transport equation of the intermittency is described as follows,

$$\frac{\partial(\rho\gamma)}{\partial t}+\frac{\partial(\rho U_j\gamma)}{\partial x_j}=P_{\gamma1}-E_{\gamma1}+P_{\gamma2}-E_{\gamma2}+\frac{\partial}{\partial x_j}\left[\left(\mu+\frac{\mu_t}{\sigma_\gamma}\frac{\partial\gamma}{\partial x_j}\right)\right] \tag{1}$$

The transition sources are calculated from Eq. 2

$$P_{\gamma1}=C_{a1}F_{length}\rho S[\gamma F_{onset}]^{C_{\gamma3}} \qquad E_{\gamma1}=C_{e1}P_{\gamma1}\gamma \tag{2}$$

where S, the strain rate magnitude, F_{length} is an empirical correlation that controls the length h of the transition region and C_{a1} and C_{e1} hold the values of 2 and 1, respectively. The destruction and re-laminarization sources are defined as follows:

$$P_{\gamma2}=C_{a2}\rho\Omega\gamma F_{turb} \qquad E_{\gamma2}=C_{e2}P_{\gamma2}\gamma \tag{3}$$

with Ω denoting the magnitude of the vorticity. The transition onset is controlled by the following functions:

$$Re_V=\frac{\rho y^2 S}{\mu} \qquad R_T=\frac{\rho k}{\mu\omega} \qquad F_{onset1}=\frac{Re_V}{2.193Re_{\theta_C}} \tag{4}$$

$$F_{onset2}=\min(\max(F_{onset1},F_{onset}^4),2.0) \qquad F_{onset3}=\max\left(1-\left(\frac{R_T}{2.5}\right)^3,0\right) \tag{5}$$

$$F_{onset}=max(F_{onset2}-F_{onset3},0) \qquad F_{turb}=e^{-\left(\frac{R_T}{4}\right)^4} \tag{6}$$

Re_{θ_C} is the critical Reynolds number where the intermittency first starts to increase in the boundary layer. This occurs upstream of the transition Reynolds number $R\tilde{e}_{\theta_C}$ and the difference between this two terms must be obtained from an empirical correlation. Both the F_{length} and Re_{θ_C}correlations are functions of $R\tilde{e}_{\theta_C}$.

The constants used in the intermittency equation are:

$$C_{a1}=2 \qquad C_{e1}=1 \qquad C_{a2}=0.06 \qquad C_{e2}=50 \qquad C_{\gamma3}=0.5 \qquad \sigma_\gamma=1.0 \tag{7}$$

The modification for separation-induced transition is:

$$\gamma_{sep}=min\left(C_{s1}\max\left[\left(\frac{Re_V}{3.235Re_{\theta_C}}\right)-1{,}0\right]F_{reattch},2\right)F_{\theta_t}$$
$$F_{reattch}=e^{-\left(\frac{R_T}{20}\right)^4} \qquad \gamma_{eff}=max(\gamma,\gamma_{sep}) \tag{8}$$

where C_{s1} is a constant with a value equal to 2.

The boundary conditions for γ at the walls indicates that the normal flow is equal to zero, while at the inlet γ is equal to 1.

The transport equation for the transition momentum thickness Reynolds number $R\tilde{e}_{\theta_c}$ is:

$$\frac{\partial(\rho R\tilde{e}_{\theta_t})}{\partial t} + \frac{\partial(\rho U_j R\tilde{e}_{\theta_t})}{\partial x_j} = P_{\theta t} + \frac{\partial}{\partial x_j}\left[\sigma_{\theta t}(\mu + \mu_t)\frac{\partial R\tilde{e}_{\theta_t}}{\partial x_j}\right] \tag{9}$$

with the source term defined as follows:

$$P_{\theta t} = C_{\theta t}\frac{\rho}{t}\left(Re_{\theta_t} - R\tilde{e}_{\theta_t}\right)(1.0 - F_{\theta t}) \qquad t = \frac{500\mu}{\rho U^2} \tag{10}$$

$$F_{\theta t} = min\left(max\left(F_{wake}e^{\left(\frac{-y}{\delta}\right)^4}, 1.0 - \left(\frac{\gamma - 1/50}{1.0 - 1/50}\right)^2\right), 1.0\right) \tag{11}$$

$$\theta_{BL} = \frac{R\tilde{e}_{\theta_t}}{\rho U} \quad \delta_{BL} = \frac{15}{2}\theta_{BL} \quad \delta = \frac{50\Omega y}{U}\delta_{BL} \quad Re_\omega = \frac{\rho\omega y^2}{\mu} \quad F_{wake} = e^{-\left(\frac{Re_\omega}{1E+5}\right)^2} \tag{12}$$

The model constants for the $R\tilde{e}_{\theta_t}$ equation are:

$$C_{\theta t} = 0.03 \qquad \sigma_{\theta t} = 2.0 \tag{13}$$

The transition model interacts with the SST turbulence model by a modification of the k equation:

$$\frac{\partial(\rho k)}{\partial t} + \frac{\partial(\rho U_j k)}{\partial x_j} = \frac{\partial}{\partial x_j}\left(\Gamma_k\frac{\partial k}{\partial x_j}\right) + G_k^* - Y_k^* + S_k \tag{14}$$

$$G_k^* = \gamma_{eff}\tilde{G}_k^* \qquad Y_k^* = min\left(\max(\gamma_{eff}, 0.1), 1.0\right)Y_k \tag{15}$$

where $\tilde{G}_k^*$ and Y_k are the original production and destruction terms for the SST model.

4. Solution Procedure

The numerical simulation of the interaction between surrounding air and solar car was achieved by using a virtual air tunnel (shown in Fig. 6) that was implemented according to the information provided by Guilmineau (2008), Guilmeneau et al. (2013) and by Ahmed (2014). The car was assumed to be at rest on top of the lower horizontal tunnel wall while the air had an incoming uniform velocity profile at the inlet with a horizontal velocity component equal to 90 km/hr. The lower moving tunnel wall had a velocity equal to 90 km/hr. At the outlet of the air tunnel a boundary condition of pressure outlet equal to zero was imposed while the remaining walls were assumed to have symmetrical boundary conditions.

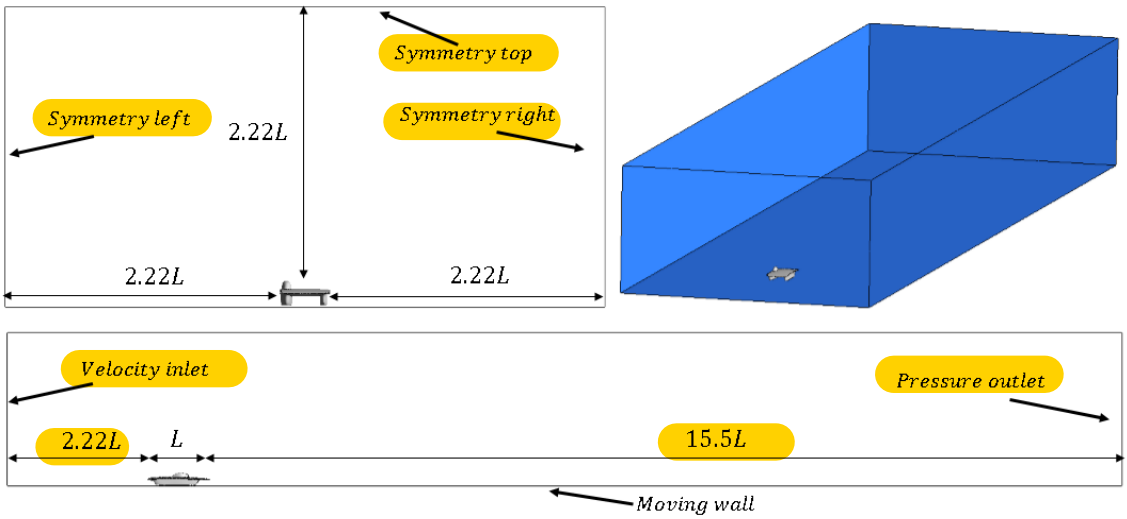

Fig. 6. Dimensions of virtual tunnel used in aerodynamic design of solar racing cars.

Domain discretization was accomplished by the Finite Volume Method, in Fluent, through successive grid refinement by keeping constant the gradients of the dependent variables between nodes. An initial mesh of about one million nodes allowed to calculate the gradients of the three velocity components, pressure, vorticity, wall shear stresses, turbulent kinetic energy and dissipation rate of turbulent kinetic energy. Successive refined meshes were built and numerical simulations were performed in order to reduce the grid size in places with larger gradients of the dependent variables, until changes in the drag coefficient between two successive meshes remained almost unchanged. Convergent results were obtained for 4 million nodes for IK1 and IK2 solar cars, while a mesh with 45 million nodes was needed for the IK3 car. Fig. 7 shows the final grid used in the fluid dynamic simulation of the three solar racing cars.

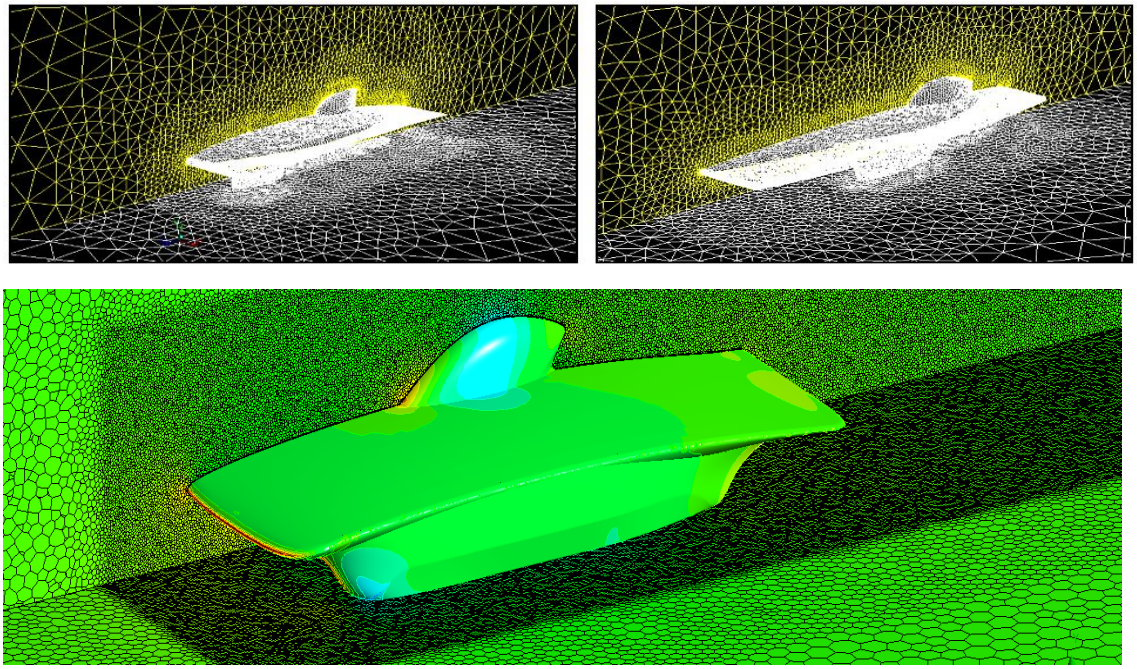

Fig. 7. Meshes for aerodynamic simulation of cars: IK1 (left), IK2 (right), IK3 (bottom).

Development of the IK3 model, with the driver seated in one side, required the study of the effect of lateral winds. The same strategy of dependent variable gradients grid refinement than in IK1 and IK2 was used. Fig. 8 depicts the IK3 solar car in the virtual tunnel. The 44 million nodes grid was built based on polyhedral and prism elements with four levels of refinements, with elements of 2 cm, 10 cm and 100 cm near the car and of a length of 1.6 m in the far away regions. Three layers of prismatic elements with a size of 1 mm were used in the air surrounding the car. The detailed information of the numerical simulation used in each car design is provided in Table 1.

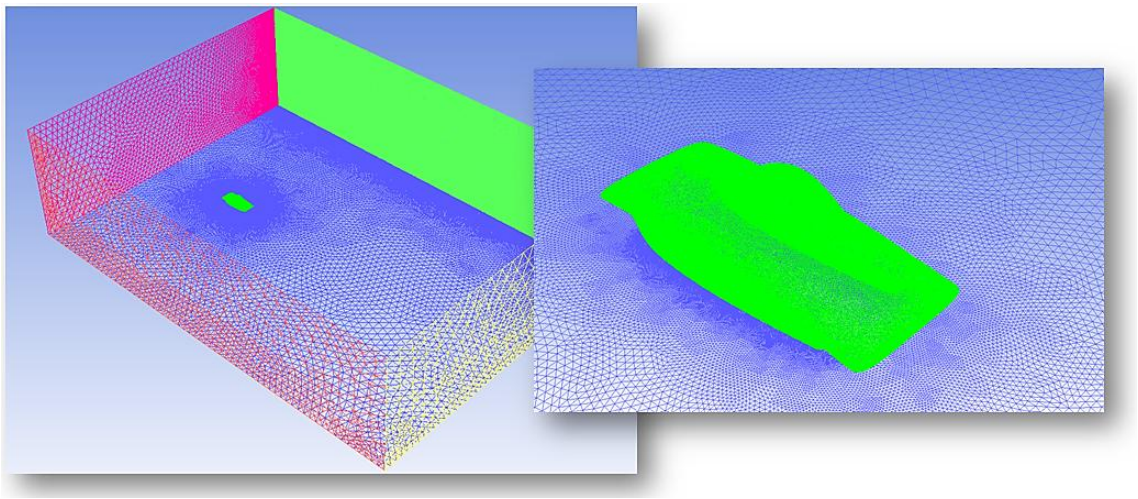

Fig. 8. Grid used in the numerical simulation of lateral wind on IK3 solar car.

Table 1. Computational information used in numerical simulations of solar racing cars.

Car model	**IK1**	**IK2**	**IK3**
Discrete volume types	tetrahedral and prisms		polyhedral and prisms
Number of nodes, millions	4	4	44
	Spatial Discretization		
Gradients	Least squares cell based		
Pressure	Standard		
Momentum	Second order upwind		
Turbulent kinetic energy	Second order upwind		
Specific dissipation rate	Second order upwind		
Intermittency	Second order upwind		
Momentum thickness Re	Second order upwind		
Convergence	Difficult to reach with initial meshes. Low under-relaxation factors are required.		Immediately, with the first mesh and using high under-relaxation factors.
CPU time (each simulation run on one i7 PC, 4770 CPU at 3.40GHz, 32Gb RAM)	50 hours of calculations and mesh adaptation. Procedure must be repeated 3 or 4 times.		From 22 to 30 hours with good convergence

5. Results and Discussion

Vehicles used in solar car races are extremely lightweights (below 250 kg) since they are powered exclusively by solar energy. The collecting solar energy area where to locate the photovoltaic cells has a limited value in each race. For these reasons the car design strategy is based on reducing the aerodynamic drag, which is known to have a much higher contribution than the rolling resistance at the typical high velocities reached during races, Ozawa et al. (1998). Therefore, the approach followed in the design of the three models of solar cars developed at ULS was based on the use of pertinent mathematical models, reliable numerical simulations and extremely resistant lower weight materials. The different systems and components were carefully studied and calculated with high accuracy: suspension, brakes, steering, battery housing and cooling system by numerical simulations with the finite element method (ANSYS). This procedure allowed weight reductions of 29% in chassis between IK2 and IK1and equivalent reduction of 20% and 25% between IK3 and IK2, while the corresponding weight reductions in suspensions accounted for 11% and 20%, respectively. The fluid mechanics of air turbulent flow around the car was described and the aerodynamic drag of each model was predicted by numerical simulations with the finite volume method (Fluent). As a main result the weight of the cars kept decreasing from 230 kg of IK1 to 184 kg of the 2013 IK2 model and finally to 165 kg in the IK3 model.

Fluid mechanics of the turbulent flow (Re = 8.56 x 10^6) around the IK1 first solar car, calculated using the κ-ϵ turbulent model, is described at the central plane in terms of the streamlines in Fig. 9. After successive variations of the car shape a refined profile was obtained in such a way that vortex generation due to the turbulent air flow was reduced as it can be observed. However, the front area of this first car was high and an elevated value of the product between de drag coefficient and the frontal area, $C_D \cdot A$, equal to 0.3 was obtained. A high drag coefficient of 0.16 that is almost half the value of a conventional car was a limiting factor of IK1 [6], but it was the winner in the category of three wheels during the Atacama Solar Car race in October, 2011, Chile, with an average velocity of 90 km/h during the race of 1082 km.

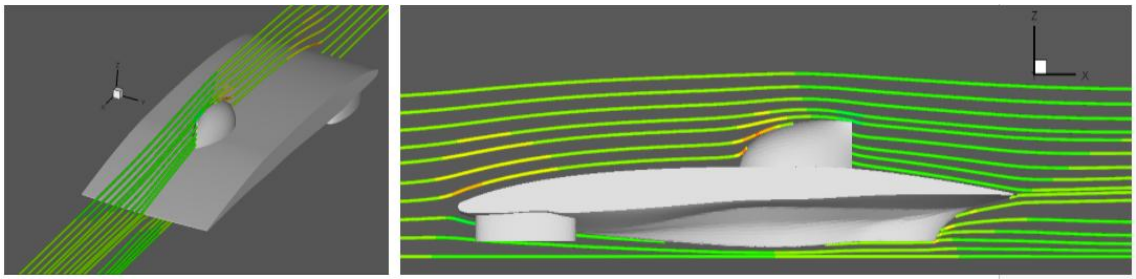

Fig. 9. Streamlines of turbulent air flow around solar car IK1, Re = 8.557.338.

The streamlines of the turbulent air flow around the second solar car, IK2, with Re = 8.39 x 10^6, depicts the fluid mechanics in Fig. 10. Flow detachment areas giving origin to a pair of vortices can be observed in the cover protecting the wheels. Adjustments in the car profile and a better design of the frontal area allowed an improvement from IK1 with a reduction that amounted to 15% in the product between the drag coefficient and the frontal area $C_D \cdot A$.

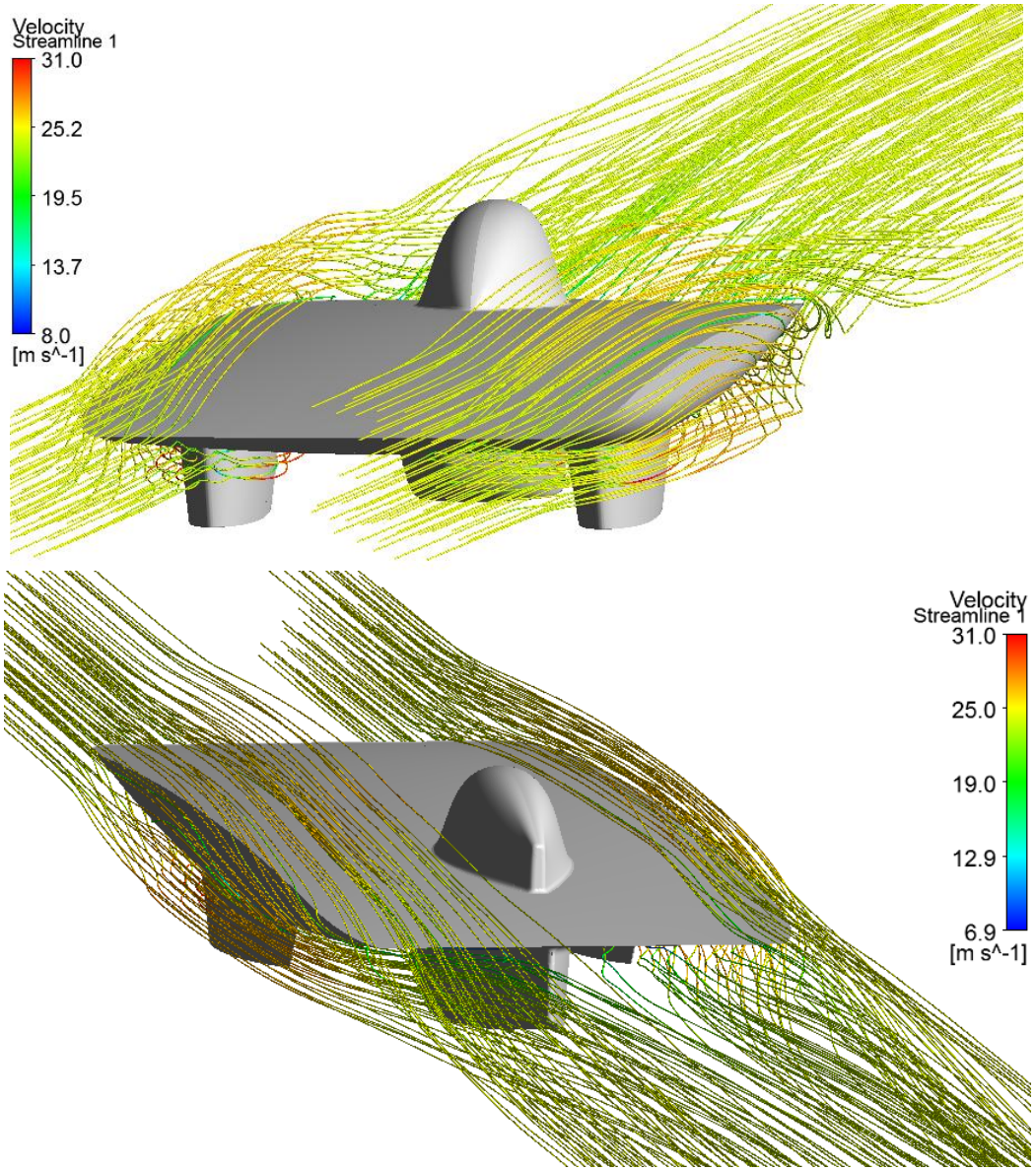

Fig. 10. Streamlines of air around the IK2 solar car, Re= 8.386.191.

The third solar car of the series, IK3, had two major differences with the two previous models: four wheels instead of three and the change of the position of the driver from the center towards one of the sides. Figure 11 shows the streamlines describing the fluid mechanics of the turbulent air flow around the solar car where turbulent vortices generated at the rear of the car can be noticed when Re = 7.7 x 10^6. The change of the driver position from the center of the car towards one of the sides reduced the frontal area in a 22%, that coupled to improvements on the car shape contour contributed to a reduction of the product of the drag coefficient and the frontal area of 54%, with a 41% reduction in the drag coefficient.

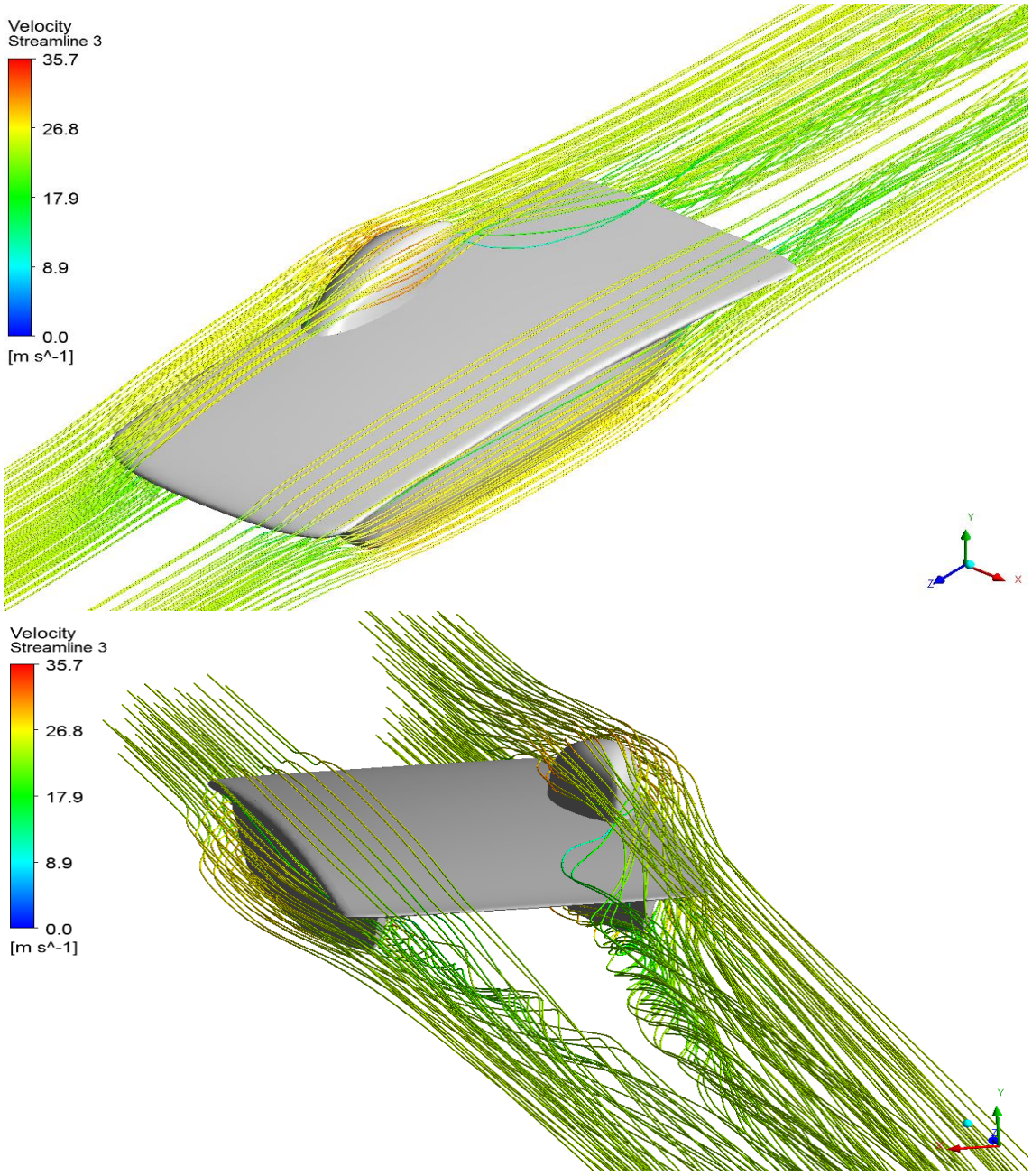

Fig. 11. Streamlines of air flow around IK3, Re=7.701.604.

A summary with the values of frontal area and drag coefficient for the successive models of solar cars is presented in Table 2. A major reduction accounting to 22% in frontal area was achieved between the 2012 model and the 2014 one that along the change in the position of the driver from the center to one of the sides contributed to a 41% reduction in the drag coefficient.

Table 2. Frontal area and drag coefficient of IK1, IK2 and IK3 solar cars.

	Frontal Area, m^2	Drag Coefficient	*Cd x A*, m^2	Reduction in Frontal Area, %	Reduction of *Cd*, %	Reduction of Cd x A, %
IK1	1.88	0.16	0.30	-	-	-
IK2	1.82	0.14	0.25	3	13	15
IK3	1.42	0.082	0.12	22	41	54

Resistive forces acting over each solar vehicle were calculated from the friction forces generated by the tires (F_r), gravity forces due to car weight (F_g) and aerodynamic drag force (F_D) using the following expressions:

$$F_r = mg\mu\cos(\alpha) \quad ; \quad F_g = mg\sin(\alpha) \quad ; \quad F_D = \frac{1}{2}\rho A C_D V^2 \tag{16}$$

Energy consumption required by each car was calculated by the resistive force, determined by adding the three forces, and multiplying the result for the car velocity. Figure 12 describes the reduction of power achieved in the three models of solar cars designed and built in 2012 (IK1), 2013 (IK2) and in 2014 (IK3) as a function of the velocity. At low velocities, below 30 km/hr, the low power required by each car was similar but at 90 km/hr, the first model (IK1) needed three times the solar energy required by the third model (IK3). The reduction of power in IK3 at high velocity was a result of the reduction of both the drag coefficient and the frontal area that resulted from a better design that included the translation of the driver from the center of the car towards one of the sides.

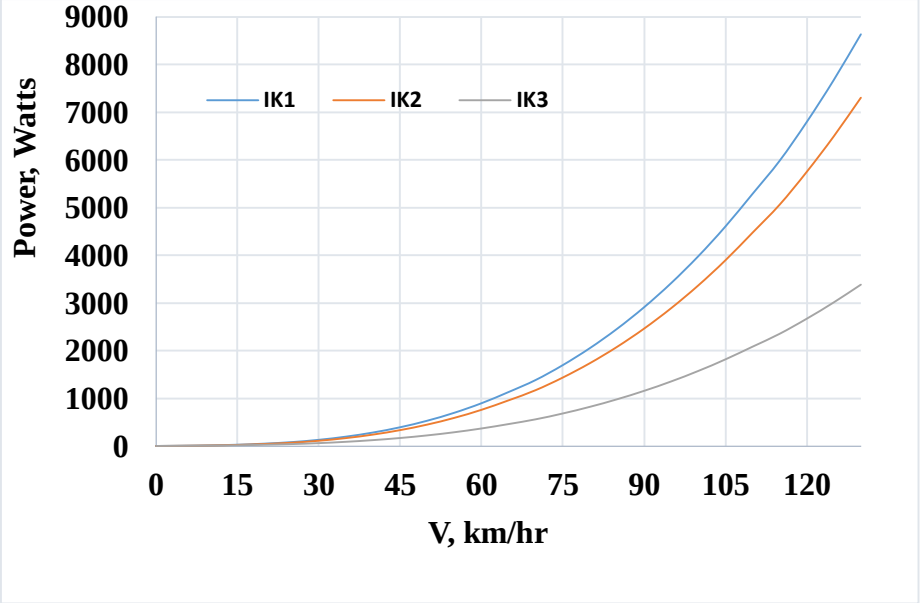

Fig. 12. Energy consumption of IK1, IK2 and IK3 cars in terms of velocity.

The energy consumption of the solar cars in a 3,000 km race, such as the World Solar Challenge in Australia, was predicted for the three models, based on the information of the route (Fig. 4). These calculations were done under the assumptions of a constant average velocity of 90 km/hr and negligible wind forces. The results for solar cars IK1, IK2 and IK3, shown in Figure 13, indicate that the improved aerodynamic design of IK2 allows a reduction of energy consumption of approximately 15%, in comparison with the previous IK1 model. The reduction of energy consumption reaches a 54% when the four wheeled IK3 is compared with the second three wheels model IK2.

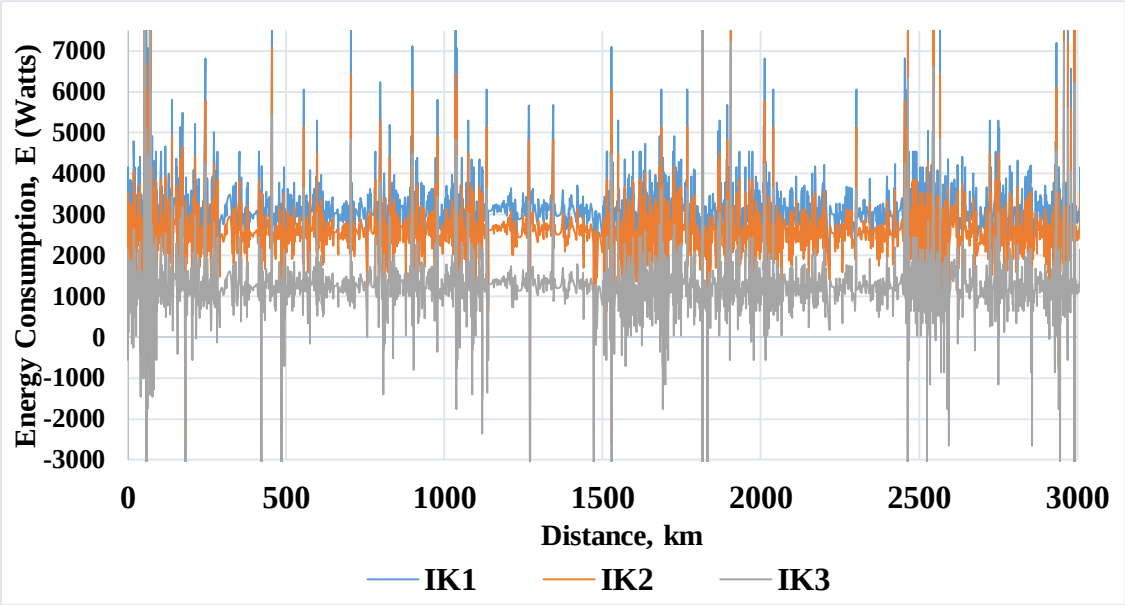

Fig. 13. Energy consumption of the three solar of cars in WSC race, Australia.

The relative influence of drag, gravitational and rolling forces acting on the IK3 solar car at a velocity of 90 km/hr in the 3000 km WSC race in Australia is presented in Fig. 14. The results indicate that 85% of the energy consumption is caused by the drag forces, while friction with the road requires a 13.5% of the solar energy captured by the solar cells and being stored in the batteries. The predicted values of energy consumption for the IK3 solar car are similar to those previously calculated for the solar Dream car that accounted to 82% in the aerodynamic drag and 18% in the friction forces by Ozawa et al. (1998).

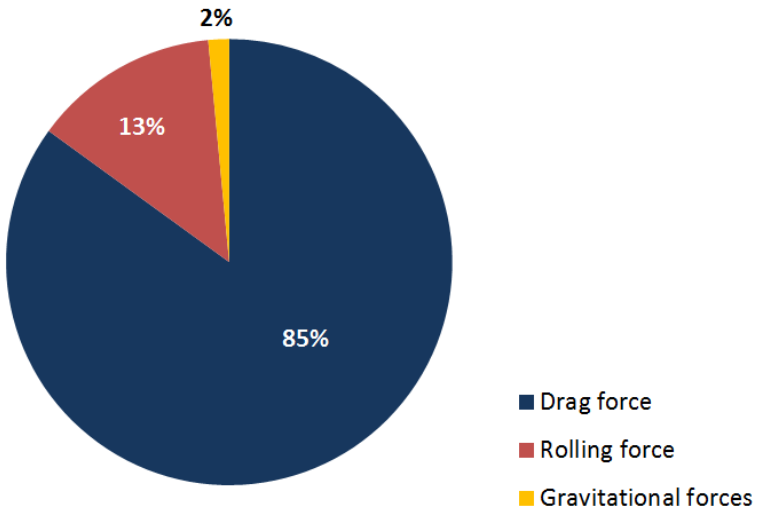

Fig. 14. Energy consumption of IK3 by drag, gravitational and rolling forces.

Effect of lateral winds on the stability of IK3 solar car.

The design of the IK3 car, with the driver seated at one side, required a careful study of effect of eventual lateral winds on its stability and on the choice of the side where the driver should be located. Lateral wind was implemented by a sinusoidal velocity profile

imposed on one of the lateral boundaries of the virtual tunnel as described in previous numerical and experimental studies of crosswinds acting on vehicles, Tsukokura et al. (2010) and Krajnovic et al. (2012). The wavelength of the sinusoidal wave was equal to 1.3L = 5.85 m and the amplitude was set at 40 km/hr, as the maximum velocity of the crosswinds to be found in WSC in Australia. Figure 15 depicts the streamlines of air around the IK3 solar car, running at 90 km/hr from north to south, as in WSC Australia, with a crosswind of 40 km/hr, from west to east at the left side of Fig. 15 (a), and from east to west at the right side, Fig. 15 (b). The lateral wind does not change the streamlines around the car when the crosswind is from west to east as it can be noticed in Fig. 15 (a), however a major change on the direction of the streamlines around the car can be observed when the crosswind is in the opposite direction, from east to west, as it is shown if Fig. 15 (b). The location of the cockpit on the right side of the car (left in Fig. 15) causes a major increment on the lateral area originating that the crosswind generates two streams one that flows over and away of the car and the second one that merge with the frontal wind. The car on the opposite side of the cockpit has a much lower lateral area and hence the wind flows over and near the top of the car merging with the frontal wind, as depicted in fig. 15 (b).

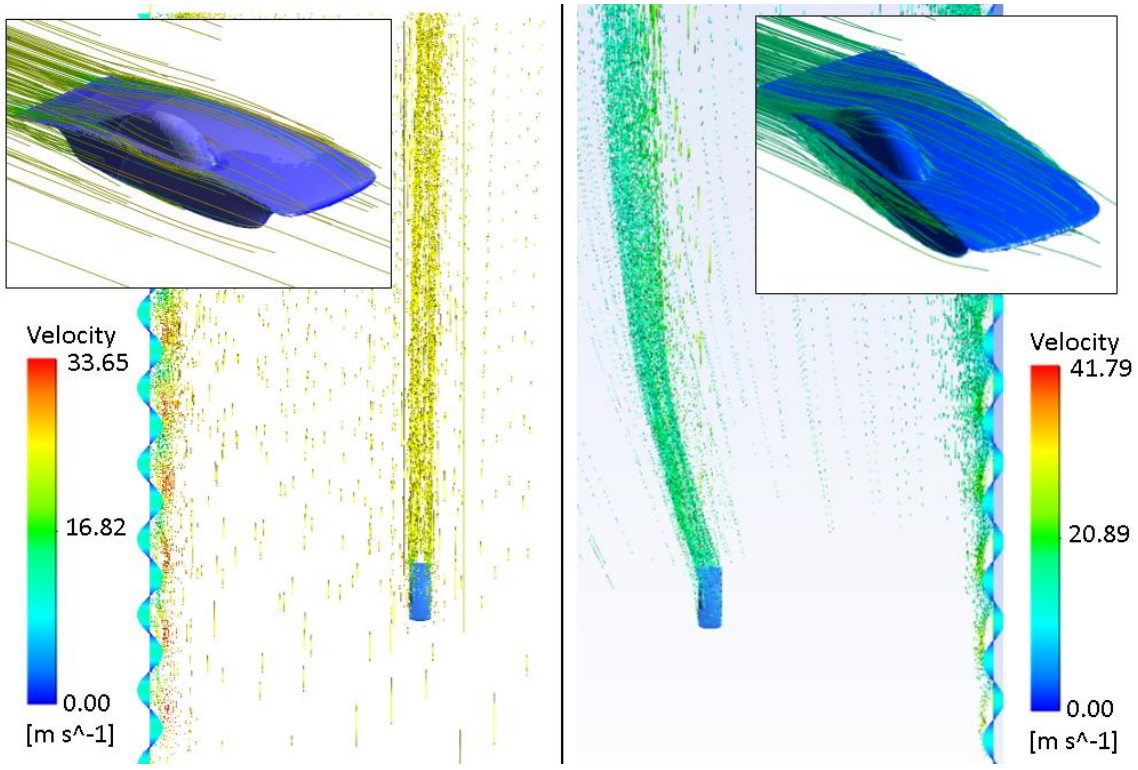

Fig. 15. Streamlines around IK3 car in virtual tunnel with lateral wind: (a) from west to east; (b) from east to west.

The effect of lateral winds, perpendicular to the car displacement, on the forces and moments, was investigated for both critical conditions: from west to east, Fig. 16 (a), and from east to west, Fig. 16 (b). Figure 16 shows the resulting forces and moments acting over the car structure of IK3 during the WSC Australia competition at an average

velocity of 90 km/hr, as caused by the coupling between the frontal from south to north wind and the lateral winds of 40 km/hr.

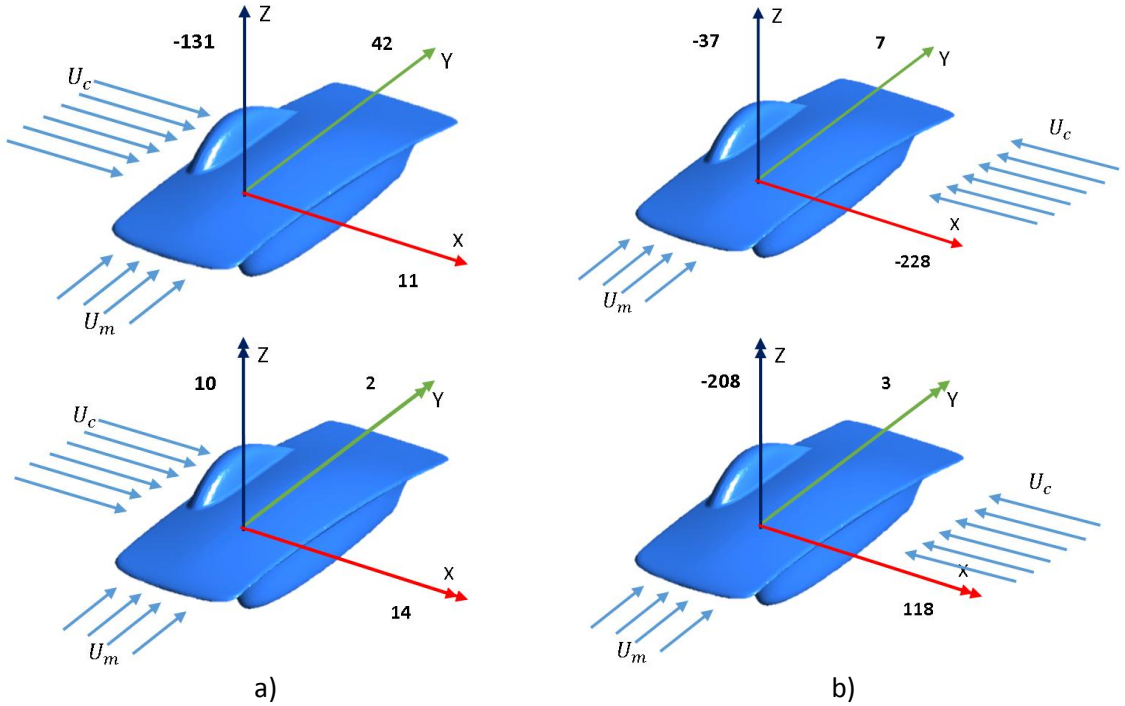

Fig. 16. Forces in N and moments in N-m on the IK3 solar car under lateral winds: (a) from the west; (b) from the east.

The results of forces and moments acting on the structure of the solar car IK3 as caused by the coupling between frontal south to north wind and a crosswind from west to east are shown in the upper and lower part of Fig. 16 (a), respectively. The cockpit located at the right side of the car generates a higher lateral area at that side giving rise to a wind flow separated from the upper surface of the car, keeping low values of forces and moments acting on the solar car. Fig. 16 (b) depicts the forces (upper part) and moments (lower section) resulting from the combined action of frontal wind and a crosswind from east to west. Lateral forces are observed to be 21 times higher than those calculated for the opposite crosswind direction, because the lateral area of the left side of the car is much smaller, and the resulting wind flows over the upper surface of the car. Drag force in south to north Y direction is six times lower than the calculated values for the opposite direction of the crosswind. The resulting force from the interaction between the front and the east to west lateral wind generates a wind flow in a diagonal direction with a higher lateral force and a lower drag force. Lift force, in Z direction, is seen to decrease 3.5 times when compared to the value obtained by the action of a lateral wind from west to east. A decrease in the lift can be dangerous because the tires grip reduces at high velocity with potential instabilities of the car, a critical situation in road curves. The pitch moment is 8.4 times higher when the lateral wind is from east to west with a potential safety hazard in descending parts of the road. The low value of the rolling moment (in Y direction) is not affected by the direction of the crosswind. The yaw moment, in Z direction, is 21 times higher when wind is from east to west with a value equal to -208 N m. The low weight of the IK3 solar car, 245

kg, that includes a driver of 80 kg, can give rise to a potential dangerous situation when a crosswind from east to west hits the car because the lift is 3.5 times lower than in the opposite wind direction. The wind magnitude and direction expected in the WSC in Australia are 40 km/hr and a north-east wind, as it was shown in Fig. 5. Fluid mechanics simulations of the turbulent flow of wind described, in Fig. 15, that the streamlines are aligned with the car direction when a crosswind of 40 km/hr is from west to east, when the pilot cockpit is located at the right side of the car.

CONCLUSIONS

Development of solar energy racing cars is a major challenge because in order to achieve a low weigh a suitable combination of highly efficient and low weigh photovoltaic cells and batteries with extreme aerodynamic design is required. The procedure of incremental improvements of aerodynamic design in a series of three models of solar racing cars have been described. Aerodynamic design was found to be the relevant parameter since aerodynamic drag accounted for 85% of the total solar energy consumption at the average race velocity of 90 km/hr.

The use of lightweight materials, photovoltaic E-60 cells with 24% of thermal efficiency, improved aerodynamic shape, cockpit at one side of the car and the use of four wheels instead of three allowed a reduction of 54% of the energy consumption between the 2011 and the 2014 solar race car models.

Aerodynamic design of solar cars can be successfully accomplished by using virtual air tunnels and Reynolds Averaged Navier Stokes models such as the transition SST turbulent model. CFD acting on solar cars can be described by the finite volume method, with discretized meshes of polyhedral and prism volumes and about 50 million nodes. Air Velocity, pressure and forces acting on the solar cars were calculated in 30 hours using an i7 PC-4770 CPU at 3.40 GHz, 32 Gb RAM.

Acknowledgements

The authors acknowledge the support of MINEDUC-Chile to Universidad de La Serena. This paper is a contribution to the *Institutional Plan on Energy Efficiency and Environmental Sustainability Improvement, ULS-1401 project*.

References

Ahmed, S.R, Ramm, G, Faltin, G., 1984. Some salient features of the time-averaged ground vehicle wake, SAE Technical Paper 840300.

Ajanovic, A., 2014. Promoting environmentally benign electric vehicles. Energy Procedia 57, 807-816.

Chen, C.J., Jaw, S.Y., 1998. Fundamentals of Turbulence Modeling. Taylor and Francis, Washington.

Corin, R.J., He, L., Dominy, R.G., 2008. A CFD investigation into the transient aerodynamic forces on overtaking road vehicle models, Journal of Wind Engineering and Industrial Aerodynamics 96, 1390-1411.

Craparo, J.C., Thacher, E.F., 1995. A solar-electric vehicle simulation code. Solar Energy 55, 221-234.

Fattori, F., Anglani, N., Muliere, G., 2014. Combining photovoltaic energy with electric vehicles, smart charging and vehicle-to-grid, Solar Energy 110, 438-451.

Flores-Sánchez, V. M., Vigueras-Zuñiga, O., Velasco-Muñoz, R., 2014 Solar vehicles design for urban use: Case adapted to Cuitláhuac Veracruz. Energy Procedia 57, 965-974.

Giannouli, M., Yianoulis, P., 2012. Study on the incorporation of photovoltaic systems as an auxiliary power source for hybrid and electric vehicles. Solar Energy 86, 441-451.

Guilmineau, E., 2008. Computational study of flow around a simplified car body. Journal of Wind Engineering and Industrial Aerodynamics 96, 1207-1217.

Guilmineau, E., Chikhaoui, O., Deng, G.B., Visonneau, M., 2013. Cross wind effects on a simplified car model by a DES approach. Computers & Fluids 78, 29-40.

Hampson, C.E., Holmes, C., Long, L.P., Piacesi, R.F.D., Raynor, W.C., 1991. The pride of Maryland: a solar powered car for GM Sunrayce USA. Solar Cells 31, 459-495.

Hemida, H., Baker, C., 2010. Large-eddy simulation of the flow around a freight wagon subjected to a crosswind, Computers & Fluids 39, 1944-1956.

Hirsch, C., 2007. Numerical Computation of Internal and External Flows, Second Ed., Elsevier, Amsterdam, p. 85.

Hung, K.S., Chao, R.M., 2012. Photovoltaic dynamic MPPT on a moving vehicle. Solar Energy 86, 1750-1760.

Jimenez, J., 2003. Computing high-Reynolds number flows: will simulations ever replace experiments. J. Turbul. 4, 22.

Kieffer, W., Moujaes, S., Armbya, N., 2006. CFD study of section characteristics of Formula Mazda race car wings. Mathematical and Computer Modelling 43, 1275-1287.

King, R.J., 1991. Solar cars race for the future results of the GM Sunrayce USA and the world solar challenge. Solar Cells 31, 395-424.

Krajnović, S., Ringqvist, P., Nakade, K., Basara, B., 2012. Large eddy simulation of the flow around a simplified train moving through a crosswind flow. Journal of Wind Engineering and Industrial Aerodynamics 110, 86-99.

Langtry, R.B., Menter, F.R., 2005. Transition Modeling for General CFD Applications in Aeronautics, AIAA Paper, Reno, Nevada.

Lehmkuhl, O., Rodríguez, I., Baez, A., Oliva, A., Pérez-Segarra, C.D., 2013. On the large-eddy simulations for the flow around aerodynamic profiles using unstructured grids, Computers & Fluids 84,176-189.

Menter F.R., Kuntz, M., Langtry, R., 2003. Ten Years of Experience with the SST Turbulence Model, in K. Hanjalic, Y. Nagano, and M. Tummers, editors: Turbulence, Heat and Mass Transfer 4, Begell House Inc..

Muyl, F., Dumas, L., Herbert, V., 2004. Hybrid method for aerodynamic shape optimization in automotive industry, Computers & Fluids 33, 849-858.

Nakashima, T., Tsubokura, M., Vázquez, M., Owen, H., Doi, Y., 2013. Coupled analysis of unsteady aerodynamics and vehicle motion of a road vehicle in windy conditions, Computers & Fluids 80, 1-9.

Ozawa, H., Nishikawa, S., Higashida, D., 1998. Development of aerodynamics for a solar race car. JSAE Review 19, 343-349.

Sagaut P., 2001. Large Eddy Simulation for Incompressible Flows. Springer Verlag, Berlin.

Tsubokura, M., Kobayashi, T., Nakashima, T., Nouzawa, T., Nakamura, T., Zhang, H., Onishi, K., Oshima, N., 2009. Computational visualization of unsteady flow around vehicles using high performance computing. Computers & Fluids 38(5), 981-990.

Tsubokura, M., Nakashima, T., Kitayama, M., Ikawa, Y., Doh, D.H., Kobayashi, T., 2010. Large eddy simulation on the unsteady aerodynamic response of a road vehicle in transient crosswinds. International Journal of Heat and Fluid Flow 31, 1075-1086.

Van Duppen, W. , 2010. Aerodynamic design of a low-drag vehicle using the interaction between Computational Fluid Dynamics and wind tunnel tests, Master Thesis, Groep T - Leuven Engineering College, KULeuven University, Belgium.

Vinnichenko, N.A., Uvarov, A.V., Znamenskaya, I.A., Ay, H., Wang, T.H., 2014. Solar car aerodynamic design for optimal cooling and high efficiency. Solar Energy 103, 183-190.

Wellington, R.P., 1996. Model solar vehicles provide motivation for school students. Solar Energy 58, 137-146.